Available online at www.sciencedirect.com
ScienceDirect
Trans. Nonferrous Met. Soc. China 33(2023) 157−167
Transactions of Nonferrous Metals Society of China
www.tnmsc.cn

Temperature dependence of compressive behavior and deformation microstructure of a Ni-based single crystal superalloy with low stacking fault energy

Wen-chao YANG[1], Peng-fei QU[1], Chen LIU[1], Kai-li CAO[1], Jia-run QIN[1], Hai-jun SU[1,2], Jun ZHANG[1], Cui-dong REN[3], Lin LIU[1]

1. State Key Laboratory of Solidification Processing, Northwestern Polytechnical University, Xi'an 710072, China;
2. Development Institute of Northwestern Polytechnical University in Shenzhen, Northwestern Polytechnical University, Shenzhen 518057, China;
3. Xi'an Aerospace Engine (Group) Co., Ltd., Xi'an 710021, China

Received 29 September 2021; accepted 31 December 2021

Abstract: The effect of temperature on the compressive behavior and deformation mechanism of a Ni-based single crystal superalloy with low stacking fault energy was investigated in the temperature range from room temperature to 1000 °C. The results indicated that both the compressive behavior and deformation microstructure were temperature-dependent. There was a higher yield strength at room temperature and then the yield strength decreased at 600 °C. After that, the yield strength would increase continuously to the maximum at 800 °C and then decrease rapidly. Furthermore, the deformation mechanisms were revealed by transmission electron microscope observation. The dislocation tangle and dislocation pairs pile-up were the main reasons for the higher yield strength at room temperature. At 600 °C, the transition in the deformation mechanisms from anti-phase boundary shearing to stacking fault shearing accounted for the slight decrease of the yield strength. At 800 °C, the deformation mechanism was mainly controlled by stacking fault shearing and the reaction of stacking faults along different directions as well as Lomer−Cottrell locks was responsible for the maximum yield strength. Above 900 °C, the primary deformation mechanism was the by-passing of dislocations, although there were still some stacking faults. Finally, the temperature dependence of deformation mechanism and compressive behavior was discussed.

Key words: Ni-based single crystal superalloy; dislocation structure; stacking fault; compressive behavior

1 Introduction

Ni-based single crystal superalloys were extensively used in the elevated temperature environments such as gas turbines and power engines due to their excellent strength, ductility, fatigue resistance, and oxidation resistance at elevated temperatures [1]. These outstanding mechanical properties were derived from their internal structure: a combination of the FCC γ matrix and the coherent $L1_2$ γ' precipitate, which was known to be the origin of unusual anomalous high-temperature mechanical properties of the superalloys [2]. Several temperature-related factors about γ' precipitates would affect the mechanical properties at various temperatures, such as the volume fraction [3], the γ/γ' lattice misfit [4−6], and the intrinsic strength [7]. And the deformation mechanism and dislocation configurations also exhibited obviously temperature-dependent [8,9]. At low temperatures, $a/2\langle 110\rangle$ dislocation pair would shear γ' precipitates and

Corresponding author: Wen-chao YANG, Tel/Fax: +86-29-88492228, E-mail: wenchaoyang@nwpu.edu.cn;
Hai-jun SU, Tel/Fax: +86-29-88492228, E-mail: shjnpu@nwpu.edu.cn
DOI: 10.1016/S1003-6326(22)66097-7

create an anti-phase boundary (APB). At intermediate temperatures, the stacking fault shearing into the γ' precipitate was the most typical feature and dislocation configurations contained stacking faults and micro-twins. And the main deformation mechanism was dislocations by-passing γ' precipitates at high temperatures.

To acquire a comprehensive property in Ni-based single crystal superalloys, more than 10 alloying elements were always added, including Co, Cr, Ti, Ta, Mo, W, Re, Ru, and so on. Among these elements in superalloys, Co was critically strategic and has attracted great attention. The addition of Co further improved the hot corrosion resistance in molten Na_2SO_4−NaCl salts [10], and it could also reduce the stacking fault energy (SFE) of γ matrix and γ' precipitates [11]. YUAN et al [12] considered that the addition of Co could improve the yield strength at intermediate temperatures. TIAN et al [13] concluded that Co addition reduced the SFE of the alloy and promoted the transition from isolated faults shearing to micro-twinning, which could enhance the yield strength and strain hardening ability at higher temperatures. Therefore, increasing Co content and reducing stacking fault energy might also improve the mechanical properties of Ni-based single crystal superalloys.

During the service, a turbine engine blade was in general subjected to a combination of surface (aerodynamic) loads, centrifugal loads, and thermal loads [14,15]. Therefore, in the operating condition of the turbine blade, besides the centrifugal tensile stress, several areas of the turbine blade, such as the contact areas between blades and the disc, would be subjected to considerable compressive stress. And the tension/compression asymmetry in yield and creep strengths was a typical feature in nickel-based single crystal superalloys [16]. Moreover, the compressive test was a basic test for many metal materials and the result was a significant reference for creep and fatigue. Tensile tests of many superalloys with various microstructures were carried out [17−20], while compressive tests were rarely reported and the mechanisms leading to their outstanding properties were still incompletely understood. Therefore, a series of compressive tests of a Ni-based single crystal superalloy with a high amount of cobalt was conducted to elucidate the compressive behavior and deformation mechanisms at different temperatures.

2 Experimental

The nominal composition of an experimental Ni-based single crystal superalloy was as follows (wt.%): 3.5Cr, 12Co, 1.5Mo, 6W, 8Ta, 4Re, 6Al, and balance Ni, and the microstructure observation indicated that the γ' phase had a low SFE about 37.2 mJ/m^2 [11]. Some single-crystal bars were directionally solidified in a modified Bridgman casting furnace as rods of 160 mm in length and 14 mm in diameter. The as-cast samples were solution heat-treated at 1290 °C, 1 h + 1300 °C, 1 h + 1310 °C, 3 h + 1320 °C, 5 h + 1328 °C, 15 h, and then air cooled. Subsequently, the solution heat-treated samples were subjected to the primary aging heat treatment for 4 h at 1180 °C and air cooling, and then were subjected to the secondary aging heat treatment for 24 h at 870 °C and air cooling. These compressive tests with a strain rate of 1×10^{-4} s^{-1} were carried out from room temperature (25 °C) to 1000 °C for the aged cylindrical specimens along the [001] direction using a thermomechanical simulator Gleeble 3500. The single crystal cylindrical specimen with a gauge length of 7 mm and a diameter of 5 mm was sectioned from single crystal bars. These samples were examined by FEI Talos F200X transmission electron microscope (TEM) under an acceleration voltage of 200 kV. Samples for TEM observation were cut into discs perpendicular to the [001] directions and mechanically ground to 60 μm and electrochemically thinned using a twin-jet polisher with an electrolyte of 7% perchloric acid in ethanol at −25 °C and 25 mA.

3 Results

3.1 Compressive behavior

The compressive curves of the experimental alloy at several typical testing temperatures are shown in Fig. 1. And these compressive true strain−stress curves at various temperatures are demonstrated in Fig. 1(a). It was clear that the experimental alloy exhibited different compressive behaviors over the experimental temperature range. At room temperature (25 °C), a typical feature of upper and lower yield points was seen on the strain−stress curve; the stress value increased as the strain increased and reached its upper yield point,

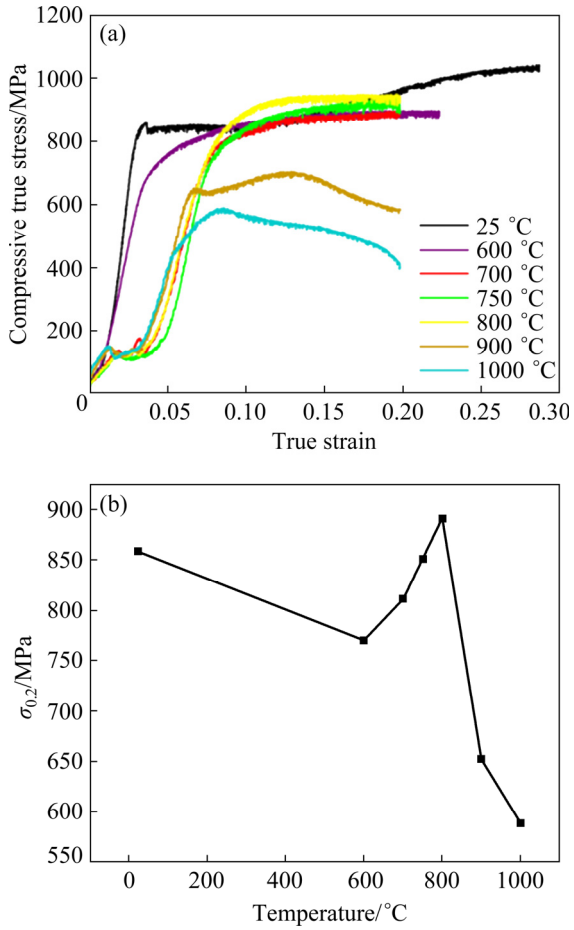

Fig. 1 Compressive curves of experimental alloy at several typical testing temperatures: (a) Compressive true strain−true stress curves at various temperatures; (b) Temperature dependence of yield strength

followed by a rapid fall in stress to its lower yield point. At 600−800 °C, the alloy exhibited similar deformation behavior, and there were no well-defined yield points; however, the work hardening still occurred during the continuous plastic deformation and the stress increased and reached a platform as the strain increased. At 900 °C, the deformation behavior of the alloy was different from that at medium and low temperatures. There were obvious yield points on the strain−stress curve. After yielding, the stress increased with the strain increasing until the ultimate stress was reached, and the stress dropped rapidly when beyond the peak load. The stress−strain curve at 1000 °C was similar to that at 900 °C, except that there was no well-defined yield point. The temperature dependence of the yield strength of the experimental alloy is demonstrated in Fig. 1(b). The yield strength at room temperature had a relatively high value, which was about 867 MPa. The yield strength gradually decreased from room temperature to 600 °C, then remarkably increased with temperature increasing and reached its maximum at 800 °C. After that, the yield strength decreased by a large margin with the temperature increasing to 1000 °C.

3.2 Deformation microstructures

Figure 2 shows the typical microstructures of the specimens after compressive deformation at low temperatures (below 600 °C). At room temperature, a large number of tangled dislocations were filled up in the γ matrix channel, as shown in Fig. 2(a). In addition to these tangled dislocations in γ matrix, another typical dislocation structure was found in γ' precipitates, and these dislocations always appeared in pairs, which indicated that pronounced APB shearing occurred during the deformation. And the pile-up of dislocation pairs in γ' precipitates was found in Fig. 2(b). At 600 °C, the dislocation pair containing an APB was the main deformation microstructure in γ' precipitates, as shown in Fig. 2(c). And the density of dislocations in the γ matrix was greatly reduced compared with that at room temperature. In addition, the stacking fault was another typical deformation microstructure in γ' precipitates, as shown in Fig. 2(d), and these stacking faults were less in number and had the same direction. In addition, some Kear−Wilsdorf (K−W) locks were also found in γ' precipitates, as shown in Fig. 2(d), and some local bulgings along superdislocation were believed to be microstructure evidence of local cross-slip motion of superdislocation from octahedral plane to cubic plane [21].

Figure 3 shows the deformation microstructures of the experimental alloy at intermediate temperatures. Figure 3(a) illustrates the deformation microstructure of the specimen at 700 °C. The shearing γ' precipitates by stacking faults dominated the deformation process at this temperature. And these stacking faults were all along the same direction, which indicated that only one ⟨112⟩ slip system was activated during compression at 700 °C. And there were little K−W locks in γ' precipitates. The microstructure at 750 °C is shown in Fig. 3(b), and some stacking faults along the same direction were also found in γ' precipitates. Interestingly, lots of dislocations were found in γ' precipitates and

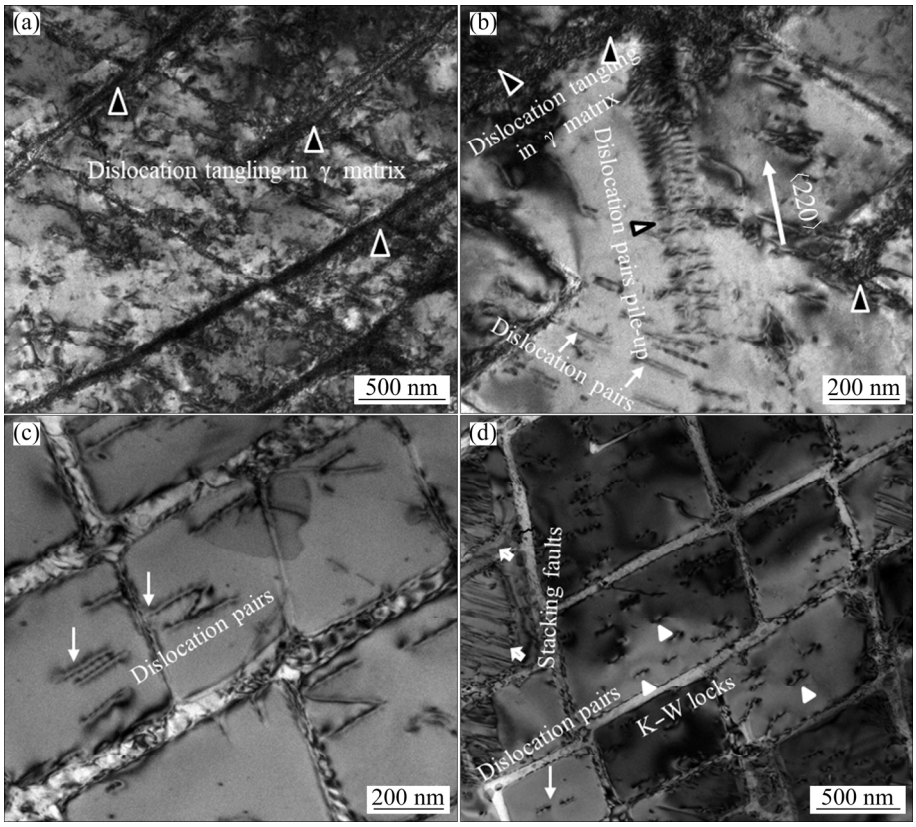

Fig. 2 TEM images showing deformation microstructures of experimental alloy at low temperatures: (a, b) RT; (c, d) 600 °C

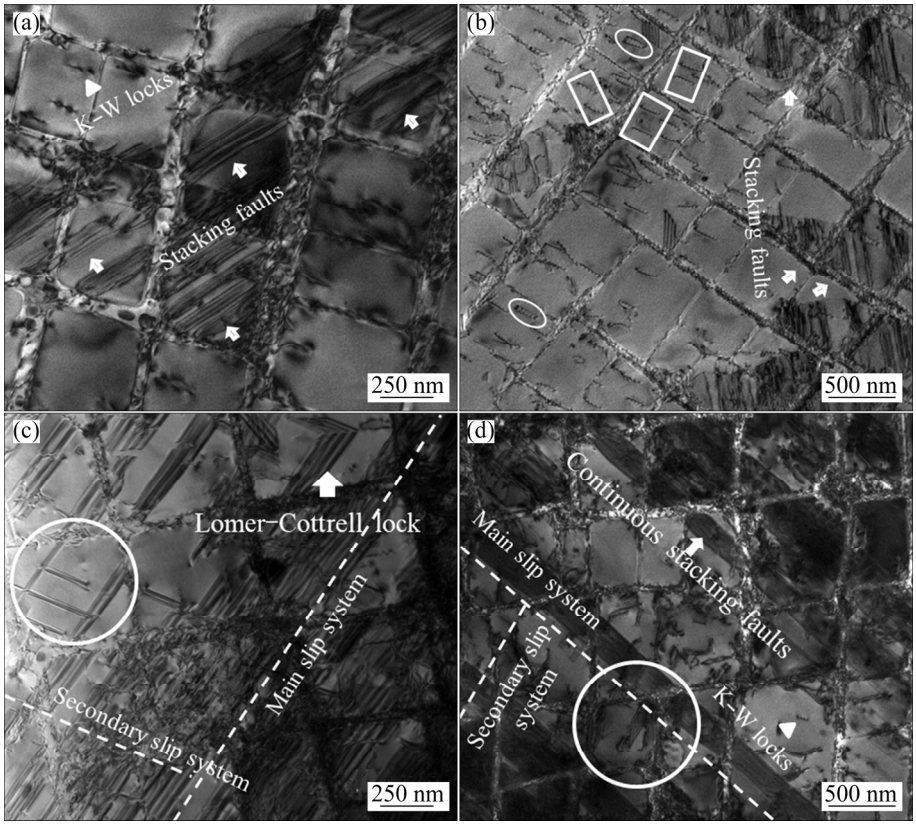

Fig. 3 TEM images showing deformation microstructures of experimental alloy at intermediate temperatures: (a) 700 °C; (b) 750 °C; (c, d) 800 °C

these dislocations existed in pairs marked by white rectangular frames. Figures 3(c, d) illustrate the deformation microstructures of the specimen at 800 °C. In Fig. 3(c), two directions of stacking faults were frequently observed in γ' precipitates, which meant that two ⟨112⟩ slip systems were activated and marked as the main and secondary slip systems according to the number and extended length of stacking faults, respectively. The number along the main slip system was higher than that along the secondary slip system, and the extended length was also larger. The Lomer−Cottrell lock was a kind of reaction structure formed by stacking fault reaction and marked in Fig. 3(c). There was another stacking fault reaction different from the Lomer−Cottrell lock, which would be marked by a white circle in Fig. 3(c). In addition, the continuous stacking fault traversing through both γ and γ' precipitates was another typical deformation characteristic at 800 °C, as shown in Fig. 3(d). And these continuous stacking faults along the main slip system would react with the stacking fault along the secondary slip system, as marked by a white circle in Fig. 3(d).

The deformation microstructures at high temperatures are shown in Fig. 4. As shown in Fig. 4(a), the coexistence of stacking fault shearing and dislocation bypassing γ' precipitates occurred at 900 °C. And these stacking faults were isolated in γ' precipitates. At 1000 °C, although there were some stacking faults in γ' precipitates, the dislocation bypassing became the main deformation mechanism, as shown in Fig. 4(b).

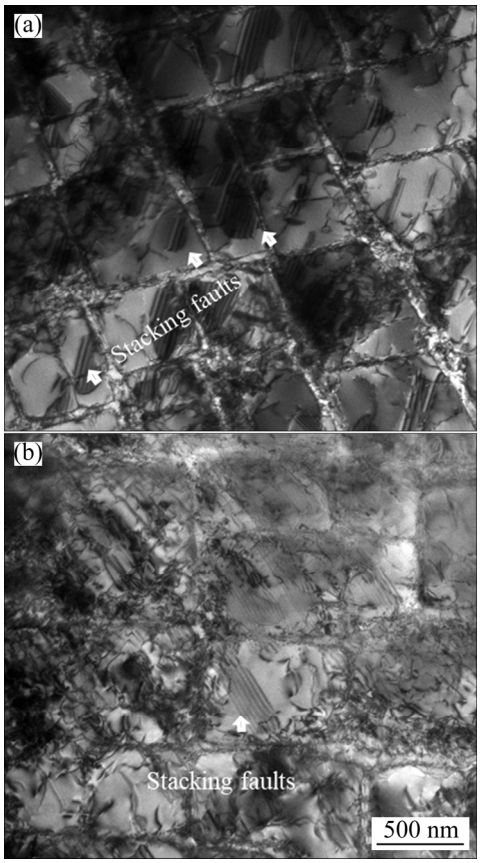

Fig. 4 TEM images showing deformation microstructures of experimental alloy at high temperatures: (a) 900 °C; (b) 1000 °C

4 Discussion

4.1 Temperature dependence of deformation mechanism

As mentioned above, the deformation microstructure was different at various temperatures. In the γ matrix, the dislocations tangling was a common feature and existed at all temperatures; however, the density of dislocations was different. And in γ' precipitates, there were several kinds of planar faults including APBs, isolated stacking faults, continuous stacking faults, and so on.

As depicted in Figs. 2(a, b), lots of tangled dislocations in the γ matrix and dislocation pairs in γ' precipitates were the typical deformation characteristics at room temperature. At the initial stage, several $a/2\langle 110\rangle$ type dislocations moved in the γ matrix and they would be blocked due to γ/γ' interface strengthening [1,22]. Then, lots of $a/2\langle 110\rangle$ dislocations with different Burgers vectors would pile up at the interface leading to dislocation tangling. As stress increased, a $a/2\langle 110\rangle$ dislocation shearing from the γ matrix into the γ' precipitate would create an APB in the γ' precipitate. The other dislocation with the same Burgers vector would remove the APB when it cut into the γ' precipitate immediately, and then a dislocation pair was created in the γ' precipitate and formed in the following way [23]:

$$a/2\langle 110\rangle + a/2\langle 110\rangle \text{ in } \gamma \rightarrow a/2\langle 110\rangle + \text{APB} + a/2\langle 110\rangle \text{ in } \gamma' \quad (1)$$

In Fig. 2(b), there were several dislocation pairs with various directions, which meant that more than two $\{111\}\langle 110\rangle$ slid systems were activated. Theoretically, eight different $\{111\}\langle 110\rangle$ slip systems would be activated for the [001] single crystal. However, due to the misorientation, some

slip systems with the larger Schmid factor were activated firstly. Moreover, the most striking feature was dislocation pairs pile-up in the γ' precipitate, which was caused by a large number of $a/2\langle 110\rangle$ dislocations with the same Burgers vector in pairs sheared into the γ' precipitate. First, a pair of $a/2\langle 110\rangle$ dislocation sheared into the γ' precipitate via Eq. (1). Then, another dislocation pair with the same Burgers vector on the same slip plane sheared into the γ' precipitate along the same direction. Due to repulsion force, the first pair would move in the γ' precipitate. When a steady stream of dislocation pairs sheared into the γ' precipitate, the former kept moving until it moved to the γ/γ' interface and encountered a dislocation tangling. Then, dislocation pairs pile-up would be created in the γ' precipitate.

Compared with room temperature, the stacking fault (SF) shearing γ' precipitates was the most striking feature at 600 °C. CARON et al [24] proposed a mechanism that these stacking faults were formed by the $a/2\langle 110\rangle$ matrix dislocation decomposition in the following way:

$$a/2\langle 110\rangle \rightarrow a/3\langle 112\rangle + \mathrm{SF} + a/6\langle 112\rangle \quad (2)$$

The $a/2\langle 110\rangle$ dislocation decomposed at the γ/γ' interface and then the leading dislocation ($a/3\langle 112\rangle$ partial dislocation) entered into the γ' precipitate and created a stacking fault, while the tailing dislocation ($a/6\langle 112\rangle$ partial dislocation) remained at the γ/γ' interface. Although the dislocation reaction (2) seemed reasonable, from the viewpoint of energy, $a/2\langle 110\rangle$ could not dissociate, as $E_{a/2\langle 110\rangle}<E_{a/6\langle 112\rangle}+E_{a/3\langle 112\rangle}$, regardless of SFE of the γ' precipitate. It needed some additional energy to keep the reaction balance and the misfit energy between the γ and γ' phases might just supply the energy [9].

Another mechanism was as follows. Two $a/2\langle 110\rangle$ dislocations with different Burgers vectors dissociated at γ/γ' interface and the decomposition reaction was described as [25]

$$a/2\langle 110\rangle + a/2\langle 110\rangle \rightarrow a/3\langle 112\rangle + \mathrm{SF} + a/6\langle 112\rangle \quad (3)$$

From the viewpoint of energy, as $E_{a/2\langle 110\rangle} + E_{a/2\langle 110\rangle} > E_{a/3\langle 112\rangle} + E_{a/6\langle 112\rangle}$, the reaction was favorable and feasible. Based on the research of stacking fault annihilation process during annealing, QU et al [26] further proved this mechanism. Therefore, this mechanism was adopted for discussion in this work.

As the temperature increased to 800 °C, the density of stacking faults continuously increased, and the dislocation pair containing an APB was reduced. In fact, the dislocation pairs shearing mechanism (APB shearing mechanism) and the stacking fault shearing mechanism were competitive during the deformation. The APB energy was considered to be nearly constant from RT to 700 °C, while the SFE decreased within the temperature range [12,27,28]. Thus, the APB shearing mechanism was favored at RT and the SF shearing mechanism was activated at 600 °C. Therefore, there was a transition of two deformation mechanisms in the temperature range of 25−600 °C, and the transition temperature was closely related to the stacking fault energy [12]. In addition, the more negative γ/γ' lattice misfit would increase the energy barrier for dislocation pairs to directly enter γ' precipitates and supply the energy for the dislocation reaction of stacking fault shearing.

At 700 °C, it should be noted that the stacking faults in Fig. 3(a) were along the same direction, indicating that only one $\{111\}\langle 112\rangle$ slip system was activated. At 750 °C, except for stacking faults along the same orientation, some short dislocations also appeared in γ' precipitates. Obviously, these dislocations existed in pairs and were parallel to each other. In addition, the blurred stacking fault contrast was found among some dislocation pairs marked by white ellipses in Fig. 3(b). Hence, they were probably stacking faults along another direction. There were three possible formation processes of these stacking faults in the γ' precipitates, as shown in Fig. 5(a). For SF-1 and SF-2, two $a/2\langle 110\rangle$ matrix dislocations with different Burgers vectors on (010) or (100) plane at the γ/γ' interface dissociated and created a stacking fault according to Eq. (3). And when viewed from the [001] orientation, $a/6\langle 112\rangle$ Shockley dislocations, b_4 and b_8, stayed at the γ/γ' interface and $a/3\langle 112\rangle$ Shockley dislocations, b_3 and b_7, sheared in the γ' precipitates. But for SF-3, two $a/2\langle 110\rangle$ matrix dislocations, b_9 and b_{10}, deposited on the upper or lower (001) plane dissociated and created a stacking fault in γ' precipitates. Although the $a/6\langle 112\rangle$ Shockley dislocation, b_{12}, still stayed at the γ/γ' interface, it seemed to be in γ' precipitates due to an inappropriate perspective. Therefore,

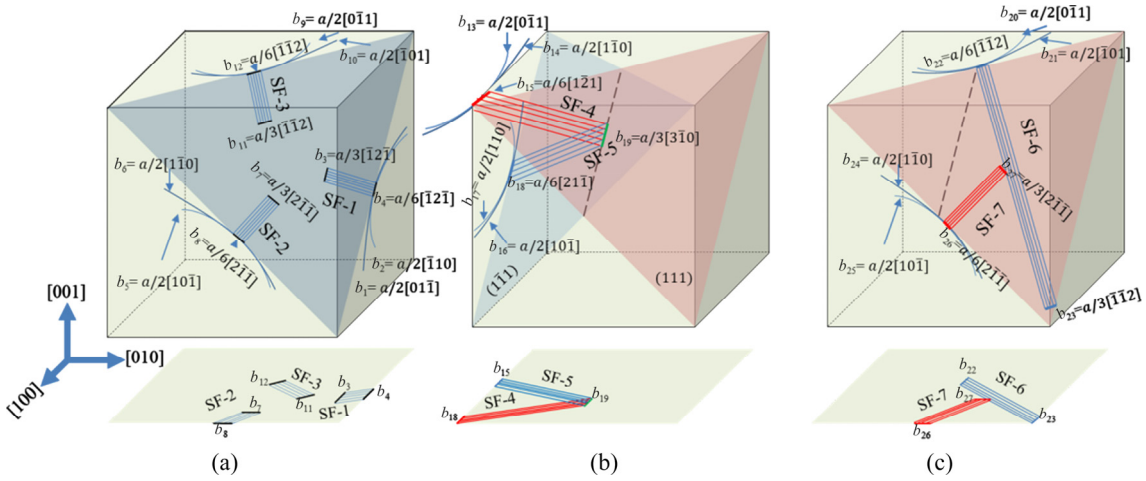

Fig. 5 Schematic illustration of formation process of several types of stacking faults: (a) Possible formation process of stacking faults; (b) Lomer−Cottrell locks; (c): Another stacking fault reaction structure

these two dislocations were $a/6\langle 112\rangle$ Shockley dislocation and $a/3\langle 112\rangle$ Shockley dislocation at both ends of the stacking fault, respectively, but stacking fault fringes were invisible.

At 800 °C, the stacking fault shearing γ' precipitates was the main deformation mechanism. At least two slip systems were activated during deformation, and interactions between different slip systems would result in different fault structures. The Lomer−Cottrell lock was a typical structure formed by stacking fault reaction [29]. A possible formation process was schematically illustrated in Fig. 5(b). Two matrix dislocations on the (111) slip plane, $b_{13}=a/2[0\,\bar{1}\,1]$ and $b_{14}=a/2[1\,\bar{1}\,0]$, dissociated at γ/γ' interface and the reaction was as follows:

$$a/2[0\,\bar{1}\,1]+a/2[1\,\bar{1}\,0]\rightarrow a/3[1\,\bar{2}\,1]+\text{SF-4}+a/6[1\,\bar{2}\,1] \quad (4)$$

The $a/3[1\,\bar{2}\,1]$ Shockley dislocation would shear into γ' precipitates and create the SF-4 on the (111) plane. At the same time, the dislocation $b_{16}=a/2[10\,\bar{1}]$ and the dislocation $b_{17}=a/2[110]$ would dissociate at γ/γ' interface and the reaction was as follows:

$$a/2[1\,1\,0]+a/2[1\,0\,\bar{1}]\rightarrow a/3[2\,1\,\bar{1}]+\text{SF-5}+a/6[2\,1\,\bar{1}] \quad (5)$$

The SF-5 was created on the $(1\,\bar{1}\,1)$ plane by the $a/3[2\,1\,\bar{1}]$ Shockley dislocation shearing. These two $a/3\langle 112\rangle$ Shockley dislocations would react at the intersection of (111) and $(1\,\bar{1}\,1)$ glide planes in the following way:

$$a/3[1\,\bar{2}\,1]+a/3[2\,1\,\bar{1}]\rightarrow a/3[3\,\bar{1}\,0] \quad (6)$$

The geometric and thermodynamic conditions could be satisfied for Eq. (6). And the line direction of the $a/3[3\,\bar{1}\,0]$ dislocation was $[10\,\bar{1}]$. Thus, the $a/3[3\,\bar{1}\,0]$ dislocation was a mixed dislocation and this type of stair−rod dislocation had been reported in the $L1_2$ phase of $Ni_{73.5}Al_9Ti_{14}Cr_{3.5}$ [30]. The $\langle 310\rangle$ stair−rod dislocation was also found in FCC metal but the Burgers vector was $a/6\langle 310\rangle$ [31]. Due to the crystal structure difference, the Burgers vector of the stair−rod dislocation in $L1_2$ γ' precipitates was different from that in FCC metal.

In addition, another structure of stacking faults reaction marked by a white circle was also found in Fig. 3(c). The density of stacking faults along the main slip system was higher and the extending length was also longer. This was because the main slip system had the largest Schmidt factor. Although another slip system would be activated owing to the lattice rotation during the plastic deformation [32], those former stacking faults would hinder the expansion of the later stacking fault. And the possible formation process was schematically illustrated in Fig. 5(c). The continuous stacking fault was also along the main slip system and hindered the expansion of other stacking faults marked by a white circle in Fig. 3(d). The SF-6 and the SF-7 were located on the same slip plane but caused by two slip systems. The $(111)[\bar{1}\,\bar{1}\,2]$ slip system had a larger Schmidt factor and was activated firstly, which resulted in the formation of SF-6 with a larger extending width. When the

$(1\,1\,1)[2\,\bar{1}\,\bar{1}]$ slip system was activated, SF-7 would be blocked by SF-6.

As the temperature increased further, the density of stacking faults decreased. Therefore, only a few stacking faults were visible in the specimens when the deformation temperature was above 900 °C. The dislocation bypassing γ' precipitates became the main deformation mechanism. More interesting, there were some stacking faults at 1000 °C, because the alloy had a low stacking fault energy [11]. And similar results were reported in other superalloys with a high amount of cobalt [33].

4.2 Temperature dependence of compressive behavior

As mentioned above, the deformation behavior was different at various temperatures and the yield strength had obvious temperature dependence. In general, the temperature dependence of deformation behavior and yield strength stemmed from several temperature-related factors, including the γ/γ' lattice misfit, the intrinsic strength of γ' precipitates, the volume fraction of γ' precipitates, the deformation mechanism, and so on. Previous investigations demonstrated that almost Ni-based single crystal superalloys had the negative γ/γ' lattice misfit and the γ/γ' lattice misfit would decrease with increasing temperature following a similar law that the γ/γ' lattice misfit slightly reduced from RT to about 700 °C and rapidly decreased above it [5,34]. Therefore, the performance below 700 °C did not originate from the change of the γ/γ' lattice misfit. The intrinsic strength of γ' precipitates was also a key factor affecting the properties. It unusually increased with an increase in temperature, reaching a peak value at approximately 800 °C, and then decreased sharply [7]. Although alloying additions would increase the intrinsic strength, the tendency was consistent and the peak value was also at intermedium temperature (700−800 °C). The volume fraction of γ' precipitates would keep at a relatively stable value at higher temperature (below 800 °C) and decrease slightly when the temperature was above 800 °C and below 1050 °C [6,35].

At room temperature, the slip system with the biggest Schmid factor would be firstly activated due to the crystal misorientation in specimens. And the strain was mainly originated from the single slip in the elastic deformation stage. After yielding, other slip systems would take place owing to lattice rotation. And interactions among these slip systems caused the formation of dislocation tangling, which were confined in the γ matrix due to the blocking of the coherent γ/γ' interface. The high-density tangled dislocation was beneficial to work hardening. In addition, some dislocation pairs with APB would shear into γ' precipitates as the interface stress increased. The dislocation pairs pile-up was another important reason for work hardening.

The yield strength at 600 °C was lower than that at room temperature, which was similar to other alloys [36]. The γ/γ' lattice misfit and the volume fraction of γ' precipitates did not affect the yield strength at 600 °C. CUI et al [9] thought that the majority of plastic deformation took place in the γ matrix at 600 °C and the decrease in strength of the γ phase might be responsible for the reduction of the yield strength from room temperature to 600 °C. However, there were fewer dislocations in the γ matrix at 600 °C, as shown in Figs. 3(c, d). In contrast, several types of dislocations sheared into γ' precipitates, causing APB and stacking faults to coexist in γ' precipitates. As the deformation temperature rose to 600 °C, the main deformation mechanism changed from APB shearing to stacking fault shearing. Moreover, the stress required for the operation of stacking fault shearing was much lower than that needed for APB shearing to occur [37]. Hence, as the deformation temperature increased from room temperature to 600 °C, the yield strength would decrease significantly.

At 700 °C, the stacking fault shearing was promoted due to the reduced γ/γ' lattice misfit and stacking fault energy. The density of stacking faults increased, which might lead to the advance of yield strength. And increasing intrinsic strength of γ' precipitates also resulted in the increase of yield strength [38]. The activation of multiple slip systems would result in lots of stacking faults with different directions at 750 °C. In addition, K−W locks were also found in γ' precipitates, which was the origination of anomalous yield [21]. Even so, the yield strength at 750 °C was still increased and the work hardening also originated from the above three factors.

At 800 °C, the experimental alloy had the maximum yield strength due to the more negative γ/γ' lattice misfit and the maximum intrinsic strength of γ' precipitates. The plenty of stacking faults (including continuous stacking faults) along

the main slip system would hinder the expansion of the stacking fault along other slip systems. Moreover, Lomer−Cottrell locks could create barriers for cross-slip, and K−W locks were also considered a reason for the maximum yield strength. Moreover, the co-segregation of Re and W in stacking faults might be beneficial to the anomalous flow behavior of γ' precipitates and then result in the maximum yield strength [39].

At temperature above 800 °C, the yield strength of the experimental alloy rapidly decreased. Although the γ/γ' lattice misfit had a more negative value, the dominant deformation mechanism was changed from shearing to bypassing above 800 °C. The intrinsic strength of γ' precipitates would decrease drastically and the volume fraction of γ' precipitates decreased slightly. Hence, the yield strength decreased continuously. In addition, some stacking faults were also found at 900 and 1000 °C, which might be the reason for work hardening.

5 Conclusions

(1) The deformation microstructure had an obvious dependence on the temperature. At low temperatures, the main deformation microstructure was dislocation pairs containing an APB. At intermediate temperatures, stacking fault shearing γ' precipitates was the main deformation mechanism and the deformation microstructure contained stacking faults in γ' precipitates, continuous stacking faults, and Lomer−Cottrell locks. The primary deformation mechanism became the dislocation bypassing of γ' precipitate above 900 °C.

(2) The compressive behavior and yield strength were also temperature-dependent. The experimental alloy had a higher yield strength at room temperature, which was mainly from the dislocation tangle in the γ matrix. And the dislocation tangle would hinder the movement of dislocation pairs in γ' precipitates and created dislocation pairs pile-up, which would result in work hardening. At 600 °C, the yield strength decreased slightly, compared with that at room temperature. Above 600 °C, the yield strength would increase as temperature increased and reached the maximum at 800 °C. Several temperature-related factors contributed to the maximum yield strength, including the more negative γ/γ' lattice misfit and the maximum intrinsic strength of γ' precipitates. In addition, the reaction of stacking faults along different directions including Lomer−Cottrell locks was another important factor. At 900 and 1000 °C, the intrinsic strength and volume fraction of γ' precipitates would decrease, which was responsible for the decrease of yield strength.

Acknowledgments

This work was funded by the National Science and Technology Major Project, China (Nos. 2017-VI-0002-0072, 2019-VI-0020-0135), the National Natural Science Foundation of China (Nos. 51771148, 52071263), the Key Research and Development Program of Shaanxi Province, China (No. 2020ZDLGY13-02), the Natural Science Basic Research Plan in Shaanxi Province, China (No. 2021JC-13), the Research Fund of the State Key Laboratory of Solidification Processing (NPU), China (No. 2021-QZ-03), the Innovation Foundation for Doctor Dissertation of Northwestern Polytechnical University, China (No. CX2021057), and the Science, Technology, and Innovation Commission of Shenzhen Municipality, China (No. JCYJ20180306171121424).

References

[1] REED R C. The superalloys fundamentals and applications [M]. Cambridge, England: Cambridge University Press, 2006.

[2] POLLOCK T M, TIN S. Nickel-based superalloys for advanced turbine engines: Chemistry, microstructure and properties [J]. Journal of Propulsion and Power, 2006, 22: 361−374.

[3] MURAKUMO T, KOBAYASHI T, KOIZUMI Y, HARADA H. Creep behaviour of Ni-base single-crystal superalloys with various γ' volume fraction [J]. Acta Materialia, 2004, 52: 3737−3744.

[4] LUO Liang, AI Cheng, MA Yue, LI Shu-sou, PEI Yan-ling, GONG Sheng-kai. Influence of temperature on the lattice misfit and elastic moduli of a Ni based single crystal superalloy with high volume fraction of γ' phase [J]. Materials Characterization, 2018, 142: 27−38.

[5] NATHAL M V, MACKAY R A, GARLICK R G. Temperature dependence of γ−γ' lattice mismatch in Nickel-base superalloys [J]. Materials Science and Engineering, 1985, 75: 195−205.

[6] DIOLOGENT F, CARON P, D'ALMEIDA T, CHAMBRELAND S, JACQUES A, BASTIE P. Temperature dependence of lattice mismatch and volume fraction of a fourth-generation monocrystalline nickel-based superalloy [J]. International Journal of Materials Research, 2006, 97: 1136−1142.

[7] THORNTON P H, DAVIES R G, JOHNSTON T L. The temperature dependence of the flow stress of the γ' phase based upon Ni_3Al [J]. Metallurgical Transactions, 1970, 1: 207−218.

[8] SMITH T M, UNOCIC R R, DEUTCHMAN H, MILLS M J. Creep deformation mechanism mapping in nickel base disk superalloys [J]. Materials at High Temperatures, 2016, 33: 372−383.

[9] CUI Lu-qing, SU Hu-hu, YU Jin-jiang, LIU Jin-lai, JIN Tao, SUN Xiao-feng. Temperature dependence of tensile properties and deformation behaviors of nickel-base superalloy M951G [J]. Materials Science and Engineering A, 2017, 696: 323−330.

[10] MENG Jun-sheng, CHEN Ming-xuan, SHI Xiao-ping, MA Qiang. Effect of Co on oxidation and hot corrosion behavior of two nickel-based superalloys under Na_2SO_4−NaCl at 900 °C [J]. Transactions of Nonferrous Metals Society of China, 2021, 31: 2402−2414.

[11] YANG Wen-chao, QU Peng-fei, SUN Jia-cheng, YUE Quan-zhao, SU Hai-jun, ZHANG Jun, LIU Lin. Effect of alloying elements on stacking fault energies of γ and γ' phases in Ni-based superalloy calculated by first principles [J]. Vacuum, 2020, 181: 109682.

[12] YUAN Y, GU Y F, OSADA T, ZHONG Z H, YOKOKAWA T, HARADA H. Deformation mechanisms in a new disc superalloy at low and intermediate temperatures [J]. Scripta Materialia, 2012, 67: 137−140.

[13] TIAN Cheng-gang, HAN Guo-ming, CUI Chuan-yong, SUN Xiao-feng. Effects of Co content on tensile properties and deformation behaviors of Ni-based disk superalloys at different temperatures [J]. Materials & Design, 2015, 88: 123−131.

[14] WITEK L. Failure analysis of turbine disc of an aero engine [J]. Engineering Failure Analysis, 2006, 13: 9−17.

[15] KAMARAJ M. Rafting in single crystal nickel-base superalloys—An overview [J]. Sadhana, 2003, 28: 115−128.

[16] WEN Zhi-xun, PEI Hai-qing, WANG Bai-zhi, ZHANG Dong-xu, YUE Zhu-feng. The tension/compression asymmetry of a high γ' volume fraction Nickel-based single-crystal superalloy [J]. Materials at High Temperatures, 2016, 33: 68−74.

[17] YANG Wan-peng, LI Jia-rong, LIU Shi-zhong, SHI Zhen-xue, ZHAO Jin-qiang, WANG Xiao-guang. Orientation dependence of transverse tensile properties of nickel-based third generation single crystal superalloy DD9 from 760 to 1100 °C [J]. Transactions of Nonferrous Metals Society of China, 2019, 29: 558−568.

[18] LIU Jin-lai, YU Jin-jiang, JIN Tao, SUN Xiao-feng, GUAN Heng-rong, HU Zhuang-qi. Influence of temperature on tensile behavior and deformation mechanism of Re-containing single crystal superalloy [J]. Transactions of Nonferrous Metals Society of China, 2011, 21: 1518−1523.

[19] GAO Shuang, HOU Jie-shan, GUO Yong-an, ZHOU Lan-zhang. Phase precipitation behavior and tensile properties of as-cast Ni-based superalloy during heat treatment [J]. Transactions of Nonferrous Metals Society of China, 2018, 28: 1735−1744.

[20] DING Han-hui, HE Guo-ai, WANG Xin, LIU Feng, HUANG Lan, JIANG Liang. Effect of cooling rate on microstructure and tensile properties of powder metallurgy Ni-based superalloy [J]. Transactions of Nonferrous Metals Society of China, 2018, 28: 451−460.

[21] TAKEUCHI S, KURAMOTO E. Temperature and orientation dependence of the yield stress in Ni_3Ga single crystals [J]. Acta Metallurgica, 1973, 21: 415−425.

[22] BENYOUCEF M, CLEMENT N, COUJOU A. TEM in situ straining of the MC2 superalloy at room temperature [J]. Philosophical Magazine A, 1995, 72: 1043−1056.

[23] BEAUCHAMP P, DOUIN J, VEYSSIÈRE P. Dependence of the antiphase boundary energy upon orientation in the L12 structure [J]. Philosophical Magazine A, 1987, 55: 565−581.

[24] CARON P, KHAN T, VEYSSIÈRE P. On precipitate shearing by superlattice stacking faults in superalloys [J]. Philosophical Magazine A, 1988, 57: 859−875.

[25] DREW G L, REED R C, KAKEHI K, RAE C M F. Single crystal superalloys: The transition from primary to secondary creep [C]//GREEN H H K A, HOWSON T E, POLLOCK T M, REED R C, SCHIRRA J J, WALSTON S. Proc Superalloys 2004. Pennsylvania, TMS, 2004: 127−136.

[26] QU Peng-fei, YANG Wen-chao, QIN Jia-run, CAO Kai-li, LIU Chen, ZHANG Jun, LIU Lin. Reveal the stacking fault shearing mechanism by its annihilation process in Ni-based single crystal superalloys [J], Materials Characterization, 2021, 180: 111419.

[27] PETTINARI F, DOUIN J, SAADA G, CARON P, COUJOU A, CLÉMENT N. Stacking fault energy in short-range ordered γ-phases of Ni-based superalloys [J]. Materials Science and Engineering A, 2002, 325: 511−519.

[28] MILLIGAN W W, ANTOLOVICH S D. The mechanisms and temperature dependence of superlattice stacking fault formation in the single-crystal superalloy PWA 1480 [J]. Metallurgical Transactions A, 1991, 22: 2309−2318.

[29] QI Dong-qing, FU Bai-dong, DU Kui, YAO Ting-ting, CUI Chuan-yong, ZHANG Jian-xin, YE Heng-qiang. Temperature effects on the transition from Lomer−Cottrell locks to deformation twinning in a Ni−Co-based superalloy [J]. Scripta Materialia, 2016, 125: 24−28.

[30] DAVID D, BONNET R. Stacking fault pyramids in the $L1_2$ phase of $Ni_{73.5}Al_9Ti_{14}Cr_{3.5}$ [J]. Philosophical Magazine Letters, 1990, 62: 89−94. (in French)

[31] LU Gang-hua, SHEN Guang-jun. Identification of a 1/6⟨310⟩ stair-rod dislocation [J]. Physica Status Solidi (a), 1981, 63: 705−710.

[32] LI Yi-fei, WANG Li, ZHANG Gong, ZHANG Jian, LOU Lang-hong. Creep anisotropy of a 3rd generation nickel-base single crystal superalloy at 850 °C [J]. Materials Science and Engineering A, 2019, 760: 26−36.

[33] ZHOU Tong-jin, DING Hong-sheng, MA Xiping, FENG Wei, ZHAO Hui-bin, LI Ai-lan, MENG Yu, ZHANG Hua-xia. Effect of precipitates on high-temperature tensile strength of a high W-content cast Ni-based superalloy [J]. Journal of Alloys and Compounds, 2019, 797: 486−496.

[34] HUANG Shen-yan, AN Ke, GAO Yan, SUZUKI A. Determination of γ/γ' lattice misfit in Ni-based single- crystal superalloys at high temperatures by neutron diffraction [J]. Metallurgical and Materials Transactions A, 2018, 49: 740−751.

[35] ROEBUCK B, COX D, REED R. The temperature

dependence of γ′ volume fraction in a Ni-based single crystal superalloy from resistivity measurements [J]. Scripta Materialia, 2001, 44: 917−921.

[36] SUN Nai-rong, ZHANG Lan-ting, LI Zhi-gang, SHAN Ai-dang. Effect of heat-treatment on microstructure and high-temperature deformation behavior of a low rhenium-containing single crystal nickel-based superalloy [J]. Materials Science and Engineering A, 2014, 606: 417−425.

[37] ZHANG P, YUAN Y, SHEN S C, LI B, ZHU R H, YANG G X, SONG X L. Tensile deformation mechanisms at various temperatures in a new directionally solidified Ni-base superalloy [J]. Journal of Alloys and Compounds, 2017, 694: 502−509.

[38] WANG G L, LIU J L, LIU J D, WANG X G, ZHOU Y Z, SUN X D. ZHANG H F, JIN T. Temperature dependence of tensile behavior and deformation microstructure of a Re-containing Ni-base single crystal superalloy [J]. Materials & Design, 2017, 130: 131−139.

[39] YI Zhou, XU Yun-lei, PENG Ping, CHEN Jiang-hua. Impact of replacement of Re by W on dislocation slip mediated creeps of γ′-Ni_3Al phases [J]. Transactions of Nonferrous Metals Society of China, 2021, 31: 2013−2023.

低层错能镍基单晶高温合金压缩行为和变形组织的温度相关性

杨文超[1]，屈鹏飞[1]，刘 晨[1]，曹凯莉[1]，秦嘉润[1]，苏海军[1,2]，张 军[1]，任翠东[3]，刘 林[1]

1. 西北工业大学 凝固技术国家重点实验室，西安 710072；
2. 西北工业大学 深圳研究院，深圳 518057；
3. 西安航空发动机(集团)有限公司，西安 710021

摘 要：在室温至 1000 ℃的范围内，研究温度对一种低层错能镍基单晶高温合金压缩行为和变形组织的影响。研究结果表明，压缩行为和变形组织均表现出温度相关性。室温下该合金具有较高屈服强度，600 ℃时屈服强度有所下降；随后，随着温度的升高，屈服强度持续增加，并在 800 ℃时达到最大值；在 800 ℃以上时，屈服强度迅速降低。通过透射电子显微镜观察揭示合金变形机制。位错缠结和位错对塞积是室温下屈服强度较高的主要原因。在 600 ℃时，变形机制从反相畴界切割向堆垛层错切割转变，这导致屈服强度略有下降。在 800 ℃时，变形机制以堆垛层错切割为主，而 Lomer−Cottrell 锁和不同方向堆垛层错之间的反应导致最大的屈服强度。在 900 ℃及以上时，虽然仍存在一些层错，但主要变形机制为位错绕过机制。最后，讨论变形机制和压缩行为的温度依赖性。

关键词：镍基单晶高温合金；位错结构；堆垛层错；压缩行为

(Edited by Bing YANG)